ELSEVIER

International Journal of Heat and Fluid Flow 22 (2001) 301–307

International Journal of HEAT AND FLUID FLOW

www.elsevier.com/locate/ijhff

Organized vortex motion in periodically perturbed turbulent separated flow over a backward-facing step

Shuya Yoshioka, Shinnosuke Obi *, Shigeaki Masuda

Department of Mechanical Engineering, Keio University, 3-14-1 Hiyoshi, Kohoku-ku, Yokohama 223-8522, Japan

Abstract

This study considers the relationship between the time-averaged and phase-averaged flow fields in turbulent backward-facing step flow under the influence of periodic perturbation. Attempts are made to clarify the interaction between organized vortex motion and turbulence statistics such as Reynolds stress. The velocity fields are measured using a particle imaging velocimeter (PIV) for three selected perturbation frequencies, one corresponding to the most effective frequency in terms of the reduction of reattachment length, one below it and another above it. The evolution of organized vortex motion due to the imposed perturbation is found remarkable except for the case of perturbation at the highest frequency, at which the organized motion dissipates so quickly behind the step that the flow is not altered. At the most effective perturbation frequency, the regions of large Reynolds stress appear as a result of strong stretching between successive vortices caused by the perturbation. It is concluded that the change in the mean velocity field due to the organized fluid motion alters the production rate of Reynolds stress, which is a key effect of the perturbation on turbulent separated flow.

Keywords: Flow separation; Periodic perturbation; Unsteady flow; Particle imaging velocimeter; Backward-facing step; Turbulence control

1. Introduction

The effect of periodic perturbation on the turbulent separated flow has been investigated in various types of flows. Even for the backward-facing step flow alone, numerous studies have been published. Their common result is that the reattachment length behind the step is remarkably reduced when the frequency of the imposed perturbation falls in a certain range. As summarized in Table 1, the most pronounced effect is obtained when the normalized perturbation frequency is close to $St \cong 0.2$, with St being the Strouhal number based on the maximum velocity and the step height. Although there are a few exceptions, the value for the optimum perturbation frequency seems to be influenced neither by Reynolds number nor by the method to realize the perturbation.

A similar tendency is found in other separated flow configurations. Attempts have been made to explain the reason for this frequency characteristic from the viewpoint of the dynamics of large-scale spanwise vortex structures in the separated shear layer (Bhattacharjee et al., 1986; Sigurdson, 1995; Chun and Sung, 1996, 1998; Kiya et al., 1997; Wu et al., 1998). On the other hand, the measured turbulence statistics indicate that the perturbation enhances the turbulent momentum transfer in the shear layer, resulting in earlier flow reattachment (Yoshioka et al., 1999). However, the relationship between vortex dynamics and the modification of the structure of turbulence field remains unexplored.

In turbulent flows associated with oscillatory motion with a known frequency, Hussain and Reynolds (1970) proposed a method of three-level decomposition: The instantaneous velocity $\hat{u}_i$ is expressed as a sum of the mean velocity U_i, a periodic component of velocity fluctuation $\tilde{u}_i$, and turbulent fluctuation u_i' as $\hat{u} = U_i + \tilde{u}_i + u_i'$. Analogously to the Reynolds-averaging practice, the momentum equations for turbulent flow with periodic oscillation are obtained by substituting the expression for instantaneous velocity in the Navier–Stokes equation and then average the whole equation over time. The resulting equation contains a term denoting the divergence of $\overline{\tilde{u}_i\tilde{u}_j}$, i.e., the cross-correlation of the periodic velocity fluctuation, and it is interpreted as the momentum transport due to organized fluid motion. The effect of the periodic perturbation imposed in the separated shear layer may be represented by this term. However, since the mean velocity field is altered by the existence of the perturbation, it is also expected that the turbulence structure changes as well. It is therefore considered that the effect of the periodic perturbation in separated flow as represented by a reduction of the reattachment length is a consequence of the combination of these two effects.

In a preceding paper (Yoshioka et al., 1999), it has been shown that the effect of the perturbation is most remarkable

* Corresponding author. Tel.: +81-45-566-1499; fax: +81-45-566-1495.

E-mail address: obsn@mech.keio.ac.jp (S. Obi).

0142-727X/01/$ - see front matter
PII: S0142-727X(01)00092-3

Notation

f_e	perturbation frequency
H	step height
P_{ij}	production rate of Reynolds stress
Re	Reynolds number, $Re = U_c H/\nu$
St	Strouhal number, $St = f_e H/U_c$
U_c	mean velocity at the center of the inlet channel
$\hat{u}_i$	instantaneous velocity, $\hat{u}_i = U_i + \tilde{u}_i + u'_i = U_i + u_i = \langle U_i \rangle + u'_i$
U_i	mean velocity component
$\tilde{u}_i$	periodically fluctuating component of velocity
u'_i	turbulent fluctuating component of velocity
u_i	fluctuating velocity component
$\overline{u_i u_j}$	Reynolds stress
v_e	injection velocity at the slit exit
V_e	amplitude of the velocity of the perturbation
x, y	Cartesian coordinates

Greeks

ϕ	phase angle of the oscillation
τ_{ij}	molecular stress
ν	kinematic viscosity

Superscripts

–	time-averaging
$\langle\rangle$	phase-averaging

Table 1
Most effective perturbation frequency for separation control in backward-facing step flow[a]

Author(s)	Method	*Re*	Expansion ratio	Optimum *St*
Roos and Kegelman (1986)	FP	3.9×10^4		0.22
Bhattacharjee et al. (1986)	EA	$2.6–7.6 \times 10^4$	1.1	0.2–0.4
Hasan and Khan (1992)	IO	3.0×10^4	1.07	0.185
Hasan (1992)	IO	1.1×10^4	1.07	0.185
Honami et al. (1993)	FP	3.85×10^4	1.5	0.200
Chun and Sung (1996)	IO	$1.3–3.3 \times 10^4$	1.5	0.25–0.275
Rhee and Sung (2000)[b]	IO	3.3×10^4	1.5	0.275
Yoshioka et al. (1999)	IO	$1.8–5.5 \times 10^3$	1.5	0.18–0.22

[a] EA: External acoustic forcing; IO: Internal oscillator; FP: Oscillating flap.
[b] Computational study.

when the increase in Reynolds shear stress is large in the time-averaged flow field. This paper introduces phase-averaging to distinguish the contribution by the periodic fluid motion and the turbulent one. Provided that vortex shedding is correlated with the introduced perturbation, the representative vortex structure can be extracted by averaging the turbulent flow field in synchronization with the period of perturbation. To this end, this study makes use of a two-dimensional particle imaging velocimeter (PIV) to capture the instantaneous vortex motion in the separated shear layer and applies phase-averaging to the data taken over time. The mechanism by which turbulence evolves is discussed in connection with the organized fluid motion that appears in the phase-averaged velocity field.

2. Experiments

The experiments were performed in a test section consisting of a backward-facing step (cf. Fig. 1) mounted in a closed-loop water channel as described in (Yoshioka et al., 1999). The channel expansion ratio at the step was 1.5, the height and span of the inlet channel were $2H$ and $12H$, respectively, with the step height $H = 20$ mm. Cartesian coordinates, x- and y-axes, were taken in the streamwise and wall-normal directions, respectively, originating from the step edge.

A slit the width of the span and 1 mm wide was opened at the step edge. The periodic perturbation was introduced through this slit as a direct, alternating suction/injection in the direction inclined 45° relative to the x-axis. Driving a piston of a syringe that was moved by a digitally controlled electronic motor generated the perturbation. The generated perturbation was designed to follow the expression:

$$v_e = V_e \sin(2\pi f_e t) = V_e \sin\phi, \quad (1)$$

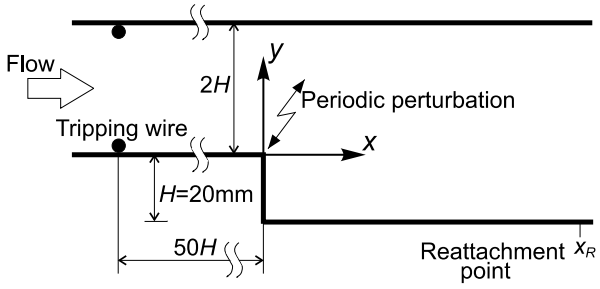

Fig. 1. Schematic of the test section.

where v_e indicates the injection velocity at the slit exit, V_e the amplitude of the velocity and f_e the frequency.

An in-house-made two-dimensional PIV was employed to measure the velocity field. The details of the instrumentation is described in an earlier paper (Yoshioka et al., 1999). To extract the organized fluid motion, a phase-averaging procedure was applied in addition to the conventional time-averaging. Due to restrictions on the data storage system, however, the results are processed only for the four representative phase angles of the perturbation, $\phi = 0,\ \pi/2,\ \pi$, and $3\pi/2$ (cf. Eq. (1)). Typically 1000 samples were used for evaluating the statistics.

The Reynolds number Re based on the mean velocity at the center of the inlet channel U_c and H was set constant to 3.7×10^3. The examination of the profile of the mean velocity and Reynolds stress has confirmed that the oncoming flow is fully developed turbulent channel flow. The amplitude of the perturbation was held at $V_e = 0.30U_c$ throughout the experiment. The frequency of the perturbation was varied to cover the most effective frequency range. The detailed velocity measurements were performed at three particular perturbation

frequencies, $St = 0.08,\ 0.19,\ 0.30$, with St being the Strouhal number, $St = f_e H/U_c$.

3. Results and discussion

3.1. Time-averaged flow field

Fig. 2 shows the time-averaged velocity vector distributions. The results are compared for the experiments with and without perturbation. The triangular mark on the bottom of each figure indicates the location where the streamwise velocity component observed along the row of measuring points nearest the wall changes its sign. The location of the triangle roughly indicates the reattachment point, although it cannot be specified accurately due to the difficulty in measuring the velocity in the vicinity of the bottom wall. The location of the flow reattachment is about $x = 5.5H$ for the experiment without perturbation (cf. Fig. 2(a)), while it shifts upstream to $x = 3.8H$ when the perturbation at $St = 0.19$ is applied (cf. Fig. 2(c)). The other two cases, $St = 0.08$ and 0.30, indicate slightly weaker effect, resulting in more moderate reduction of the reattachment length from that obtained without perturbation.

As discussed by Yoshioka et al. (1999), the shorter reattachment length is a consequence of the enhancement of momentum transfer by the imposed perturbation, which appears as an increase in the Reynolds stress component $-\overline{uv}$ that represents the transport of the streamwise component of momentum in the transverse direction. The argument is supported by the production rate of the Reynolds stress component of concern

$$P_{12} = -\overline{v^2}\frac{\partial U}{\partial y} - \overline{u^2}\frac{\partial V}{\partial x}$$

the distribution of which is presented in Fig. 3. It is clear that the imposed perturbation contributes to the increase in the Reynolds stress, as its production rate is larger for the conditions with the perturbation than that without it. The difference in the perturbation frequency appears in the magnitude and the location of maximum value of P_{12} . The most pronounced increase found in the case of the perturbation at $St = 0.30$ suggests that the more remarkable and more rapid increase of $-\overline{uv}$ behind the step is provided by the higher perturbation frequency. It may follow that the perturbation with the higher frequency provides stronger effects and hence results in the shorter reattachment length. However, this is contradictory to the findings shown in Fig. 2. The intensity of $-\overline{uv}$ is not solely determined by the production rate, but by the balance of production, dissipation, redistribution to other components and spatial transport due to diffusion. Hence, it is more straightforward to examine the total amount of Reynolds shear stress itself to clarify the influence of the perturbation. Here, the integrated Reynolds shear stress flux F_{12} that is defined by

$$F_{12} = \frac{1}{U_c^3 H}\int_{-H}^{2H} U\cdot(-\overline{uv})\,\mathrm{d}y,$$

represents the left-hand side of the transport equation for Reynolds stress and therefore accounts for the balance among all effects appearing on the right-hand side of the transport

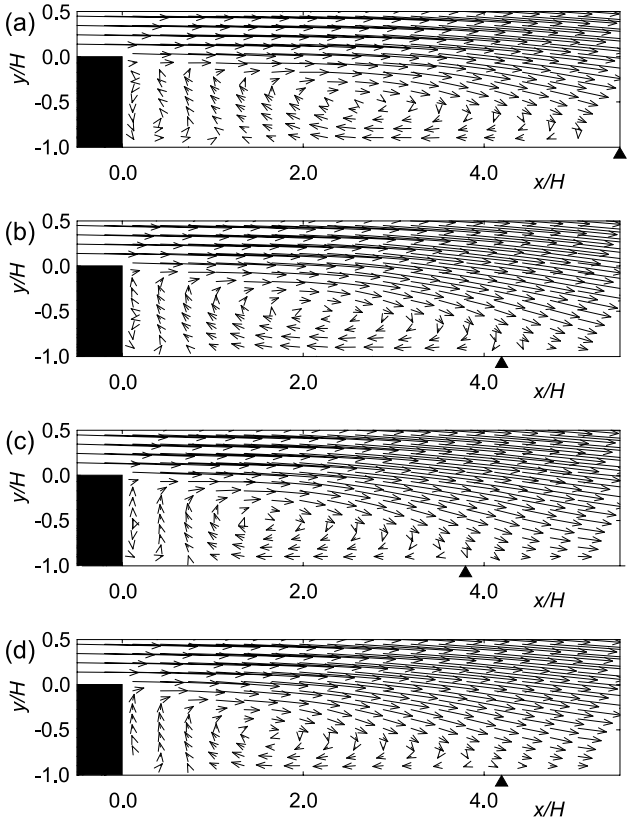

Fig. 2. Time-averaged velocity vector distribution: (a) without perturbation, and (b) perturbation at $St = 0.08$, (c) $St = 0.19$, (d) $St = 0.30$.

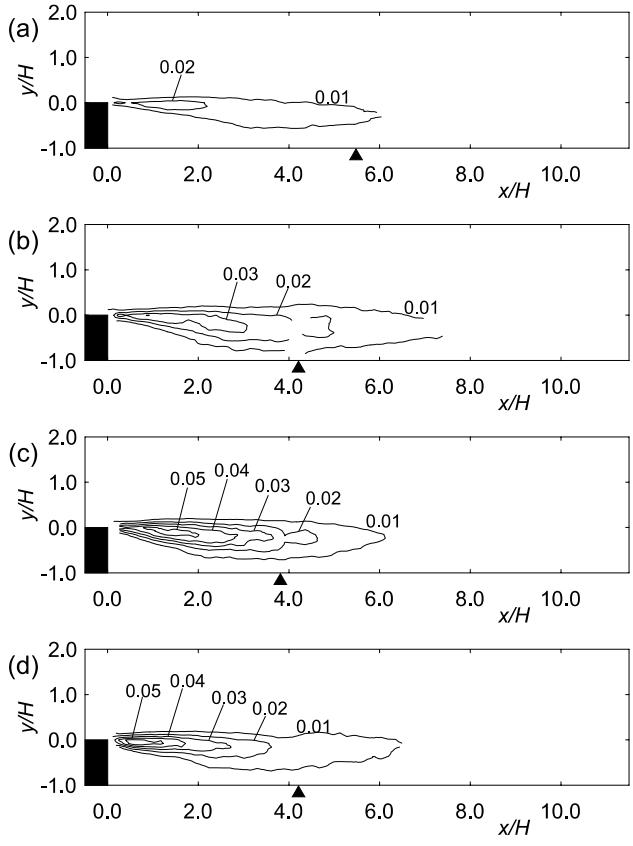

Fig. 3. Production rate of $-\overline{uv}$: (a) without perturbation, perturbation at (b) $St = 0.08$, (c) $St = 0.19$, (d) $St = 0.30$.

equation. Besides, integrating over the cross-section and neglecting the diffusion transport in the x-direction against that in y-direction, one can isolate the imbalance in the source terms of the $-\overline{uv}$ equation from the transport terms. The streamwise variation of F_{12} is presented in Fig. 4, comparing all cases. It is obvious that the perturbation indeed increases the value of $-\overline{uv}$ from the original state, though its streamwise development and its dependency on the perturbation frequency differs from what has been observed in the distribution of P_{12}. Namely, the largest value is achieved by the lowest frequency, $St = 0.08$ (indicated by open circles), near the streamwise location $x/H \approx 6.0$, where roughly three times more turbulent shear stress is transported compared to the flow without perturbation (solid line). It is noteworthy that the most effective perturbation frequency in terms of the reduction of the reattachment length, $St = 0.19$ (closed circles), does not provide the highest peak. Instead, the increase in F_{12} immediately behind the step provided by this perturbation is most remarkable among all the cases. The perturbation at the highest frequency, $St = 0.30$, yields the weakest influence on the flow as a whole, which contradicts to the observation of the P_{12} distribution. The results imply that the fluid motion caused by the perturbation at higher frequency provides a strong dissipation at the same time, so that the evolution of $-\overline{uv}$ does not occur.

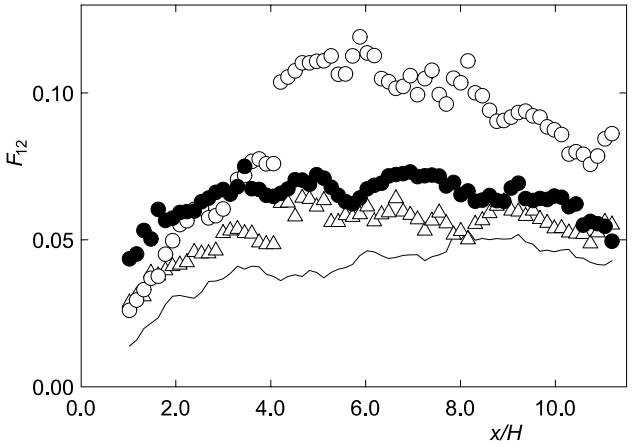

Fig. 4. Streamwise variation of the net transport of $-\overline{uv}$. Solid line; without perturbation, ○; $St = 0.08$, ●; $St = 0.19$, △; $St = 0.30$.

3.2. Phase-averaged flow field

The streamline pattern evaluated from the phase-averaged velocity field is shown in Fig. 5, where the results at the lowest frequency, $St = 0.08$, are illustrated; the four graphs represent the four perturbation phase angles in sequence. At each instant, the wavy streamline patterns are observed. Correlated to the wavy patterns, closed streamline patterns are developed behind the step. They travel downstream, as denoted by the dashed lines, at a velocity roughly equal to $0.3U_c$. The closed-loop pattern disappears near the time-averaged reattachment point. As a consequence, the time-averaged recirculation region behind the step is divided into a few closed streamline patterns at any instant of the phase-averaged field. When disturbed by the perturbation $St = 0.19$ shown in Fig. 6, the

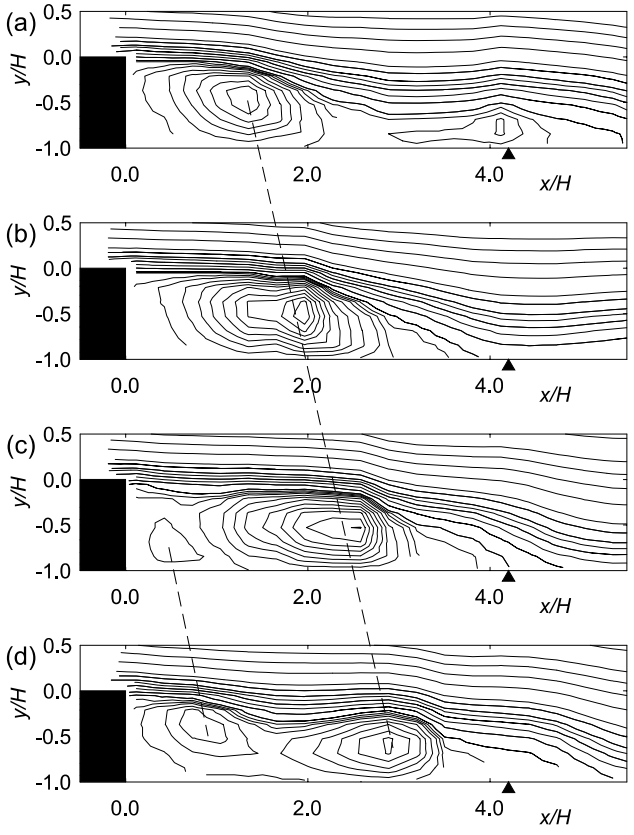

Fig. 5. Phase-averaged streamline at $St = 0.08$: (a) $\phi = 0$; (b) $\phi = \pi/2$; (c) $\phi = \pi$; (d) $\phi = 3\pi/2$.

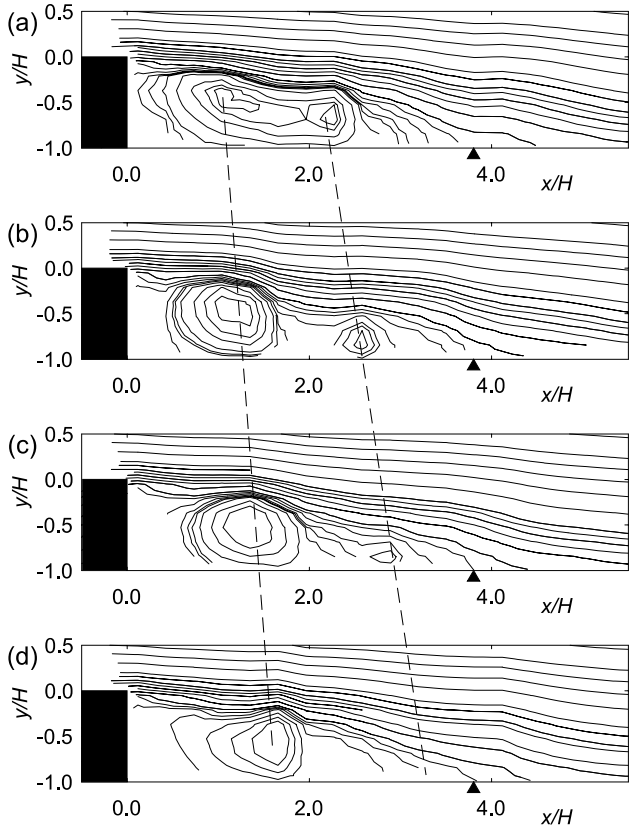

Fig. 6. Phase-averaged streamline at $St = 0.19$: (a) $\phi = 0$; (b) $\phi = \pi/2$; (c) $\phi = \pi$; (d) $\phi = 3\pi/2$.

wavy patterns of the streamline and the associated closed-loops are also observed, but the wavelength of the streamline is shortened compared to the former case. Under this condition, the number of vortices per unit time existing in the recirculation region is increased and there are at least two closed-loop patterns at any instant.

3.3. Phase-averaged Reynolds shear stress

When ensemble averaging in synchronization to a known frequency is applied to the Navier–Stokes equation, the equation for fluid motion associated with the perturbation at constant frequency is obtained

$$\frac{\partial}{\partial t}\rho\langle u_i\rangle + \frac{\partial}{\partial x_j}\rho\langle u_i\rangle\langle u_j\rangle = -\frac{\partial\langle p\rangle}{\partial x_i} - \frac{\partial}{\partial x_j}\rho\langle u_i' u_j'\rangle + \frac{\partial}{\partial x_j}\langle\tau_{ij}\rangle, \qquad (2)$$

where $\langle\tau_{ij}\rangle$ is molecular stress related to the ensemble-mean strain-rate tensor. By analogy to Reynolds stress in the steady turbulent flow field, it is natural to interpret the phase-averaged product of the fluctuating velocity components, the second term on the right-hand side of Eq. (2), as the additional momentum transfer due to turbulent motion. Unlike the Reynolds stress in steady flow, this quantity is a function of time or of the phase angle ϕ and is called the phase-averaged Reynolds stress herein.

The distribution of the phase-averaged Reynolds shear stress as evaluated from the experiment for the perturbation at $St = 0.08$ is presented in Fig. 7. Only the shear stress component $-\langle u'v'\rangle$ is considered here. The dashed lines in the figure are the trace of the streamline pattern indicated in Fig. 5. As a whole, the distribution of $-\langle u'v'\rangle$ resembles that of $-\overline{uv}$ in the experiment without perturbation, though a few distinctive features exist: There are menisci in the contour behind the step and they are located between the dashed lines, indicating that the phase-averaged Reynolds stress travels with the streamline patterns. In the case with the perturbation frequency at which the reattachment length is reduced the most, $St = 0.19$ shown in Fig. 8, the local-maximum regions of the phase-averaged Reynolds shear stress are more densely distributed compared with those in the case of $St = 0.08$.

To shed light on the relationship between the turbulent field and the periodic perturbation, the production rate of the phase-averaged Reynolds stress was investigated next. In analogy to the Reynolds stress equation, one can derive the transport equation for the phase-averaged Reynolds stress. The production rate appearing in the resulting equation is expressed as:

$$\langle P_{12}\rangle = -\langle v'^2\rangle\frac{\partial\langle u\rangle}{\partial y} - \langle u'^2\rangle\frac{\partial\langle v\rangle}{\partial x}.$$

Figs. 9 and 10 show the distribution of $-\langle P_{12}\rangle$ at $St = 0.08$ and $St = 0.19$, respectively. In the case of $St = 0.19$, the distribution of $-\langle P_{12}\rangle$ seems to be similar to that of $-\langle u'v'\rangle$ (cf. Fig. 8) indicating that the phase-averaged Reynolds stress is indeed generated by this term. The resemblance between the distribution of the Reynolds stress and that of the production rate is remarkable in the location of maxima which are located between the two neighboring vortices behind the step (denoted by the dotted lines, cf. Fig. 6). The region between two neighboring vortices is characterized by significant strain fields and hence remarkable production of Reynolds stress, which is compared to the "braids" appearing between two

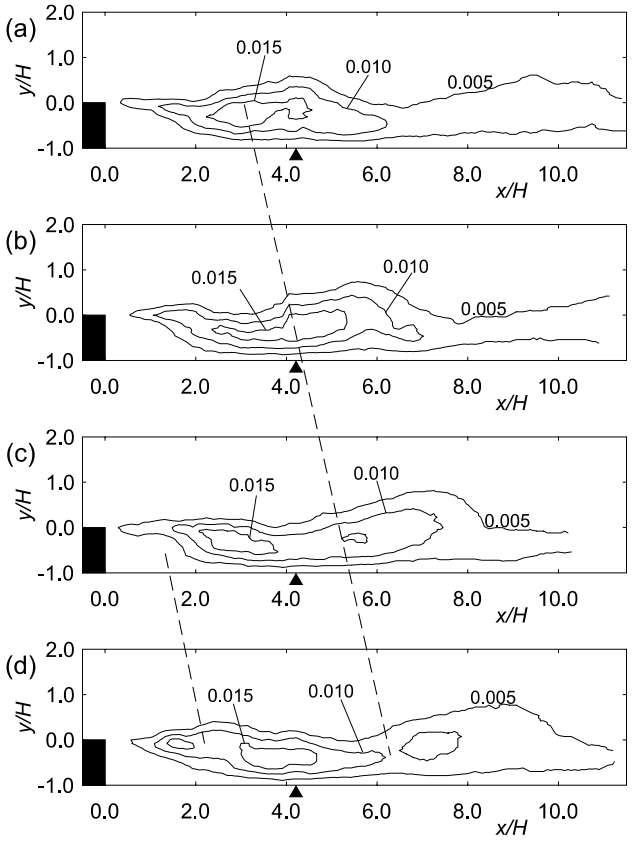

Fig. 7. Phase-averaged Reynolds shear stress $-\langle u'v'\rangle/U_c^2$ at $St = 0.08$: (a) $\phi = 0$; (b) $\phi = \pi/2$; (c) $\phi = \pi$; (d) $\phi = 3\pi/2$.

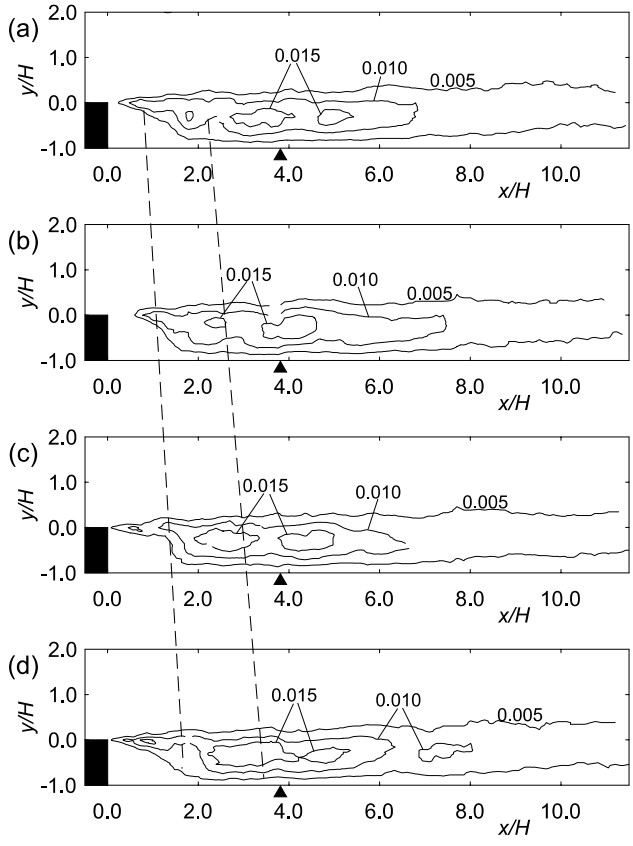

Fig. 8. Phase-averaged Reynolds shear stress $-\langle u'v'\rangle/U_c^2$ at $St = 0.19$: (a) $\phi = 0$; (b) $\phi = \pi/2$; (c) $\phi = \pi$; (d) $\phi = 3\pi/2$.

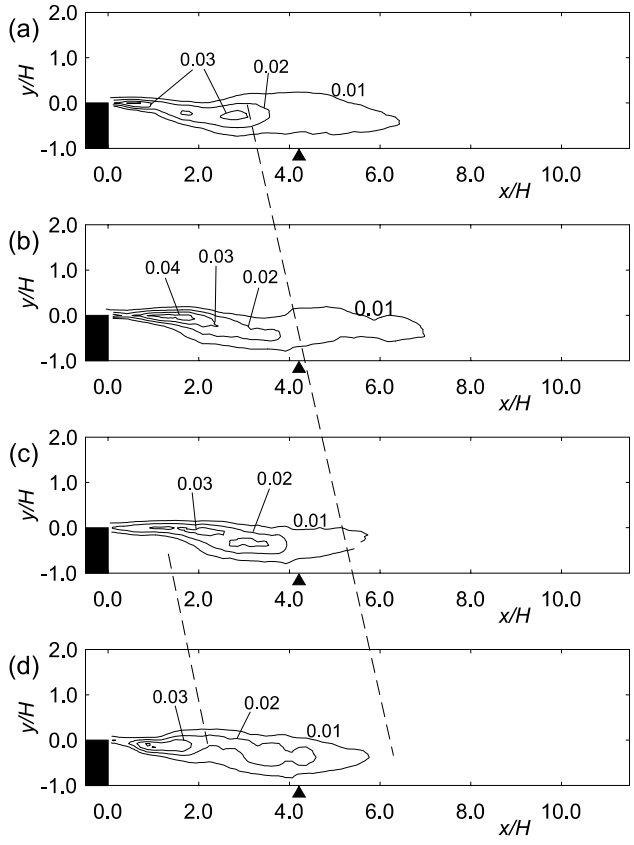

Fig. 9. Phase-averaged production rate of Reynolds shear stress $-\langle P_{12}\rangle \cdot H/U_c^3$ at $St = 0.08$: (a) $\phi = 0$; (b) $\phi = \pi/2$; (c) $\phi = \pi$; (d) $\phi = 3\pi/2$.

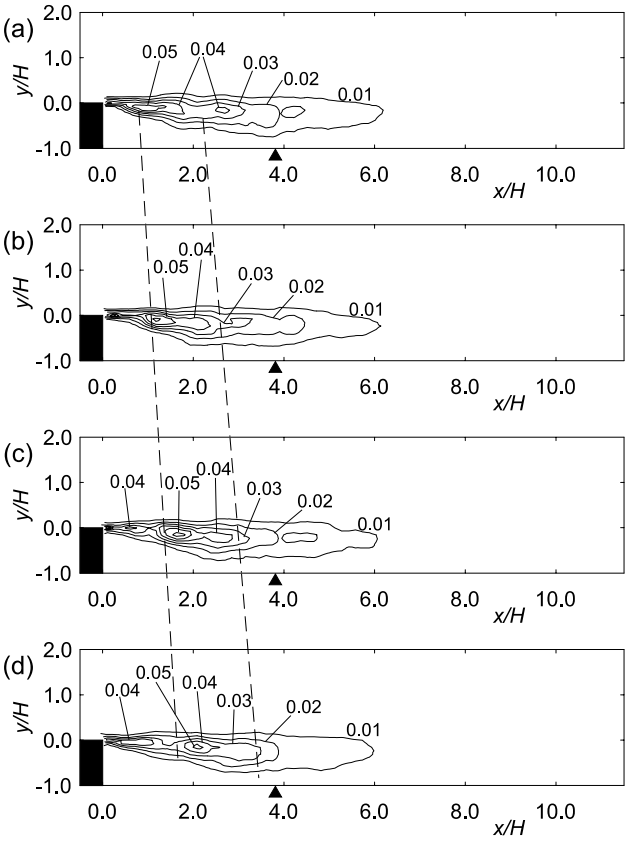

Fig. 10. Phase-averaged production rate of Reynolds shear stress $-\langle P_{12}\rangle \cdot H/U_c^3$ at $St = 0.19$: (a) $\phi = 0$; (b) $\phi = \pi/2$; (c) $\phi = \pi$; (d) $\phi = 3\pi/2$.

co-rotating vortices of a free mixing layer (e.g., Caulfield and Kerswell, 2000). The above observation points to the existence of an indirect effect of the periodic perturbation, i.e., the increase of Reynolds stress is realized by the ensemble-mean vortex pattern due to the imposed perturbation. The same tendency is also observed in the $St = 0.08$ case shown in Fig. 9. The only difference compared to the higher frequency case is the number density of vortices existing behind the step. The interaction between the imposed perturbation and the spanwise roller-and-braid structure that develops immediately behind the step (Neto et al., 1993) is considered to be of primary importance in determining the frequency characteristics, though the lack in spectral information hinders the decisive conclusion to be drawn within the framework of the present experiment.

In general, the above-mentioned indirect effect of the periodic perturbation is less appealing compared to the direct effect, i.e., the periodic fluid motion itself. However, a similar experiment conducted in turbulent flow in an asymmetric plane diffuser indicates that the magnitude of these two effects varies with the perturbation frequency; the indirect effect plays an equally important role as the direct one under the condition at which the perturbation realizes its maximum effect (Obi et al., 1997). This experiment corresponds to this condition and it is interesting to estimate these two individual effects separately. However, the presently available data set is too sparse to perform the time-averaging of the phase-averaged quantities with sufficient accuracy. Nevertheless, this result points to the fact that the interaction of the organized vortex structure generated by the perturbation provides the additional production of turbulent fluid motion, and it is considered to be an important mechanism of momentum transfer enhancement in this kind of flow.

4. Conclusion

The relationship between turbulence statistics and oscillatory, organized fluid motion is experimentally investigated in the periodically perturbed turbulent separated flow over a backward-facing step. The velocity fields are measured by a PIV and phase-averaging procedure is introduced to extract the fluid motion that is synchronized with the perturbation. The promotion of the flow reattachment in time-averaged flow is well correlated with the increase in the production of Reynolds shear stress. The phase-averaged flow field reveals that the organized fluid motion exists in the separated shear layer. The region with strong deformation appears between the vortex structures, which promote the production of Reynolds stress. The consequent enhancement of momentum transfer is considered to be an important effect of the periodic perturbation imposed on the turbulent separated flow.

Acknowledgements

Part of this study is supported by the Ministry of Education though a Grant-in-Aid for Scientific Research. The authors are grateful to Professor K. Nishino of Yokohama National University, Professor K. Hishida and his co-workers of Keio University for their valuable advice on PIV measurements.

References

Bhattacharjee, S., Scheelke, B., Troutt, T.R., 1986. Modification of vortex interactions in a reattaching separated flow. AIAA Journal 24, 623–629.

Caulfield, C.P., Kerswell, R.R., 2000. The nonlinear development of three-dimensional disturbances at hyperbolic stagnation points: a model of the braid region in mixing layers. Physics of Fluids 12, 1032–1043.

Chun, K.B., Sung, H.J., 1996. Control of turbulent separated flow over a backward-facing step by local forcing. Experiments in Fluids 21, 417–426.

Chun, K.B., Sung, H.J., 1998. Visualization of a locally-forced separated flow over a backward-facing step. Experiments in Fluids 25, 133–142.

Hasan, M.A.Z., Khan, A.S., 1992. On the instability characteristics of a reattaching shear layer with nonlaminar separation. International Journal of Heat and Fluid Flow 13, 224–231.

Hasan, M.A.Z., 1992. The flow over a backward-facing step under controlled perturbation: laminar separation. Journal of Fluid Mechanics 238, 73–96.

Honami, S., Shizawa, T., Tsuchitani, H., 1993. Organized structures in the reattachment process in a backward-facing step flow. In: Proceedings of the Ninth Symposium on Turbulent Shear Flows, P108.

Hussain, A.K.M.F., Reynolds, W.C., 1970. The mechanics of an organized wave in turbulent shear flow. Journal of Fluid Mechanics 41, 241–258.

Kiya, M., Shimizu, M., Mochizuki, O., 1997. Sinusoidal forcing of a turbulent separation bubble. Journal of Fluid Mechanics 342, 119–139.

Neto, S.S., Grand, D., Métais, O., Lesieur, M., 1993. A numerical investigation of the coherent vortices in turbulence behind a backward-facing step. Journal of Fluid Mechanics 256, 1–25.

Obi, S., Ishibashi, N., Masuda, S., 1997. The mechanism of momentum transfer enhancement in the periodically perturbed turbulent separated flow. In: Hanjalić, K., Peeters, T.W.J. (Eds.), Turbulence, Heat and Mass Transfer, vol. 2. Delft University Press, Delft, pp. 835–844.

Rhee, G.H., Sung, H.J., 2000. Numerical prediction of locally forced turbulent separated and reattaching flow. Fluid Dynamics Research 26, 421–436.

Roos, F.W., Kegelman, J.T., 1986. Control of coherent structures in reattaching laminar and turbulent shear layers. AIAA Journal 24, 1956–1963.

Sigurdson, L.W., 1995. The structure and control of a turbulent reattaching flow. Journal of Fluid Mechanics 298, 139–165.

Wu, J.Z., Lu, X.Y., Denny, A.G., Fan, M., Wu, J.M., 1998. Post-stall control on an airfoil by local unsteady forcing. Journal of Fluid Mechanics 371, 21–58.

Yoshioka, S., Obi, S., Masuda, S., 1999. Momentum transfer in the periodically perturbed turbulent separated flow over the backward-facing step. In: Banerjee, S., Eaton, J.K. (Eds.), Turbulence and Shear Flow Phenomena-1. Begell House, Inc., pp. 1321–1326.